Physical and chemical properties of lunar magma

van Kan, M.

2011

Chapter 7

Trace element partitioning between ilmenite, armalcolite and anhydrous silicate melt: implications for the formation of lunar high-Ti mare basalts

Mirjam van Kan Parker, Paul R. D. Mason, Wim van Westrenen

Submitted to: Geochemica et Cosmochemica Acta

ABSTRACT

We performed a series of experiments at high pressures and temperatures to determine the partitioning of a wide range of trace elements between ilmenite, armalcolite and anhydrous lunar silicate melt, to constrain geochemical models of the evolution of the interior of the Moon. Experiments yielding partition coefficients were performed in graphite-lined platinum capsules at pressures and temperatures ranging from 1.1 to 2.3 GPa and 1300-1400 °C using a synthetic Ti-enriched Apollo 'black glass' composition in the CaO-FeO-MgO-Al_2O_3-TiO_2-SiO_2 system. Trace element partition coefficients (D) for both ilmenite and armalcolite show highly incompatible values for the rare earth elements (REE, $D_{La}^{\text{Ilm-melt}}$ 0.0020 ± 0.0010 to $D_{Lu}^{\text{Ilm-melt}}$ 0.069 ± 0.010 for ilmenite and $D_{La}^{\text{Arm-melt}}$ 0.0048 ± 0.0023 to $D_{Lu}^{\text{Arm-melt}}$ 0.041 ± 0.008 for armalcolite) with the light REE slightly more incompatible compared to the heavy REE. The high field strength elements vary from highly incompatible for Th, U and to a lesser extent W (for ilmenite: $D_{Th}^{\text{Ilm-melt}}$ 0.0013 ± 0.0008, $D_{U}^{\text{Ilm-melt}}$ 0.0035 ± 0.0015 and $D_{W}^{\text{Ilm-melt}}$ 0.039 ± 0.005, and for armalcolite $D_{Th}^{\text{Arm-melt}}$ 0.008 ± 0.003, $D_{U}^{\text{Arm-melt}}$ 0.0048 ± 0.0022 and $D_{W}^{\text{Arm-melt}}$ 0.062 ± 0.03), to mildly incompatible for Nb, Ta, Zr, and Hf (e.g. $D_{Hf}^{\text{Ilm-melt}}$ 0.28 ± 0.05 and $D_{Hf}^{\text{Arm-melt}}$ 0.76 ± 0.07). Both ilmenite and armalcolite fractionate the high field strength elements as $D_{Ta} > D_{Nb}$ and $D_{Hf} > D_{Zr}$. Values for D_{Ta}/D_{Nb} and D_{Hf}/D_{Zr} are comparable for ilmenite between 1.3 and 1.6 and for armalcolite 1.3 and 1.4. Armalcolite is slightly more efficient at fractionating Hf from W during lunar magma ocean crystallisation, with D_{Hf}/D_{W} = 11.9-12.9 compared to 6.7-7.5 for ilmenite. The transition metals vary from mildly incompatible to compatible, with the highest compatibilities for Cr in ilmenite (D ~7.5) and V in armalcolite (D ~8.1). D values show no clear variation with pressure in the small range covered.

Crystal lattice strain modelling of D values for di-, tri- and tetravalent trace elements shows that in ilmenite, divalent elements prefer to substitute for Fe while armalcolite data suggest REE replacing Mg. Tetravalent cations appear to preferentially substitute for Ti in both minerals, with the exception of Th and U that likely substitute for the larger Fe or Mg cations. Lattice strain models of

trivalent element partitioning data do not show unequivocally which substitution mechanism dominates.

Our data enable us to model the Lu-Hf-Ti systematics of lunar high-Ti mare basalts. We show that their subchondritic Lu/Hf ratios and high TiO_2 contents require preferential dissolution of ilmenite or armalcolite from late-stage, lunar magma ocean cumulates into low-Ti partial melts of deeper pyroxene-rich cumulates.

1. INTRODUCTION

Ilmenite (nominal composition $FeTiO_3$) and armalcolite ($(Fe,Mg)Ti_2O_5$) are important titanium-rich, oxide minerals found on the Moon (e.g. Lucey et al., 2006). In contrast to the relatively minor role ilmenite plays in most terrestrial magmatic processes, it is thought to have played a crucial role in the late stages of lunar magma ocean (LMO) crystallisation and subsequent mare basalt formation (e.g. Snyder et al., 1992; Shearer and Papike, 1999). Petrological modelling shows that ilmenite becomes a stable phase late during LMO crystallisation. Its presence at relatively shallow levels combined with its relatively high density (Tronche et al., 2010) is thought to have resulted in a gravitationally unstable mineral stratification in the lunar mantle (e.g. Snyder et al., 1992), inducing a large-scale mantle overturn triggering significant lunar basalt formation (e.g. Lee et al. 2002; Hess and Parmentier, 1995; de Vries et al., 2010).

Quantifying the major and trace element partitioning behaviour of both ilmenite and armalcolite during partial melting and crystallisation processes at different pressure *(P)* and temperature *(T)* conditions, is essential when constraining their involvement in LMO crystallisation and mare basalt generation using geochemical modelling. For example, crystallisation of ilmenite has been suggested as the primary reason for the observed fractionation of W from Hf in lunar samples (Righter and Shearer, 2003; Klemme et al., 2006). Ilmenite has also been invoked to explain the low Lu/Hf ratios in high-Ti bearing mare basalts (e.g. Nakamura et al. 1986; Beard et al., 1998).

Recently, Thacker et al. (2009) examined the *P-T* stability fields of ilmenite and armalcolite in the interior of the Moon, as well as the major element distribution between these Ti-rich minerals and co-existing silicate melt. However, to date, very little is known about the distribution of trace elements between ilmenite and/or armalcolite and (anhydrous) silicate melt. Previously published studies (Green et al., 1971; McKay and Weill, 1976; Palme and Wlotzka, 1977; Irving et al., 1978; Fujimaki et al., 1984; McKay et al., 1986; Nakamura et al., 1986; Candela and Bouton, 1990; Latourrette et al., 1991; Stimac and Hickmott, 1994; Zack and Brumm, 1998; Klemme et al., 2006) reporting ilmenite-melt and/or armalcolite partition coefficients show large variations in measured D values (Fig. 1). These variations are related to a combination of the range of natural and synthetic compositions (x) used, and differences in the P, T and fO_2 conditions applied,

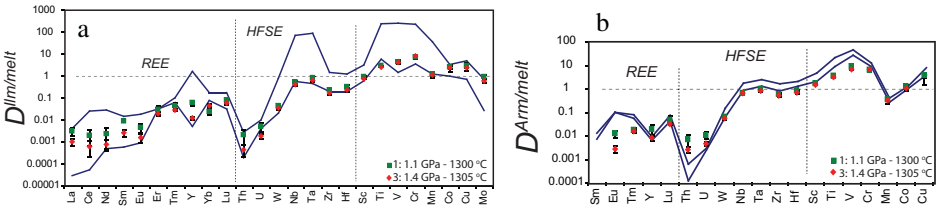

Figure 1. Compilation of partition coefficients D_i for Ilm/Gk **a**) and Arm **b**) determined in this study and literature data (shown as lines representing upper and lower limits). For Armalcolite not all experimentally determined D's from this study are included since no literature data was available for comparison for many elements. Literature generally uses Ilmenite while generally Ilmenite-Geikielite minerals were studied. For armalcolite trace element partitioning data presented in Klemme et al. (2006) for ferropseudobrookite was incorporated when a MgO was present. Data are from Green et al. (1971), McKay and Weill (1976), Palme and Wlotzka (1977), Irving et al. (1978), Fujimaki et al. (1984), McKay et al. (1986), Nakamura et al. (1986), Candela and Bouton (1990), Latourette et al. (1991), Stimac and Hickmott (1994), Zack and Brumm (1998), Klemme et al. (2006). For Er (Ilm-Gk) and Eu (Arm) only one study was available, therefore minimum and maximum values are equal.

make it very difficult to identify appropriate *D* values for petrogenetic modelling of lunar (or terrestrial) melting and crystallisation processes involving these minerals. The absence of systematic data also preclude development of a predictive thermodynamic partitioning model as was done previously for other minerals including clinopyroxene (Wood and Blundy, 1997) and garnet (Draper and van Westrenen, 2007; van Westrenen and Draper, 2007).

Here we present a series of ilmenite-melt and armalcolite-melt partition coefficients for large ion lithophile elements (LILE) Li and Ba; rare earth elements (REE) La, Ce, Nd, Sm, Eu, Er, Tm, Y, Yb, and Lu; high field strength elements (HFSE) Zr, Nb, Hf, Ta, Th and U; and transition metals Sc, V, Mn, Co, Cu, and Mo, derived from experiments performed in a synthetic lunar basaltic composition at a temperatures between 1300 and 1400 °C and *P* between 1.1 and 2.3 GPa. The wide range of trace elements that were added allows us to assess the applicability of the crystal lattice strain model (Blundy and Wood, 1994) for both ilmenite- and armalcolite-melt for the first time, providing a step towards the development of fully predictive partitioning models. We illustrate the relevance of our new data by assessing the roles of ilmenite and armalcolite in determining the Lu-Hf-Ti systematics of high-Ti lunar mare basalts.

2. METHODS

2.1 Experimental and analytical techniques

Experiments were performed in the CaO-FeO-MgO-Al_2O_3-TiO_2-SiO_2 system (CFMATS). The starting mixture and experimental *P-T* conditions were guided by the study of Beck and Hess (2004), who mapped the solubility of ilmenite in a synthetic high-Ti Apollo red glass. Our starting mixture (Table 1) was chosen to be a synthetic Ti-enriched high-Ti Apollo black glass equivalent (Delano, 1986).

Table 1. Major element composition (in wt%) of average Apollo 14 black (A14) glass (Delano, 1986) and of the synthetic six-component starting material (SM) used in this study. *n.* denotes the number of microprobe analysis used to determine the SM composition.

	n.	SiO_2	TiO_2	Al_2O_3	Cr_2O_3	FeO	MgO	MnO	CaO	Na_2O	K_2O	Total
A14		*34*	*16.4*	*4.6*	*0.92*	*24.5*	*13.3*	*0.31*	*6.9*	*0.23*	*0.16*	*101.32*
SM	*6*	30.4(4)	25.3(3)	4.18(6)	-	21.7(2)	11.7(1)	-	6.33(8)	-	-	99.6(2)

Numbers in parentheses indicate one standard deviation (1σ) of replicate analyses in terms of last significant numbers: 30.4(4) should be read as 30.4 ± 0.4.

The starting material was prepared by mixing appropriate amounts of high purity (99.5-99.99 %, Alfa Aesar) powdered oxides (MgO, Fe_2O_3, Al_2O_3, TiO_2, SiO_2) and $CaCO_3$ (99.95-100.05 %, Alfa Aesar). The oxides MgO, Al_2O_3, TiO_2 and SiO_2 were fired overnight at 1000 °C prior to use to drive off residual moist, and subsequently stored at 110 °C, as were Fe_2O_3 and $CaCO_3$. After mixing the starting material under ethanol in an agate mortar for one hour, it was dried in air and decarbonated in a Pt crucible in a box furnace by gradually raising *T* from 650 to 1200 °C over seven and a half hours. The Pt crucible had previously been iron-saturated to minimize Fe loss during starting composition preparation. The mixture was subsequently molten at 1550 °C for 10 minutes and quenched by immersing the bottom of the Pt crucible in water. A small chip of the resulting glass was embedded in epoxy, polished, carbon coated and analysed for homogeneity by electron microprobe.

The resulting glass was ground under ethanol in an agate mortar for one hour and doped with varying amounts of the LILE Li and Ba; the REE La, Ce, Nd, Sm, Eu, Er, Tm, Y, Yb, and Lu; the HFSE Zr, Nb, Hf, Ta, Th and U; and transition metals Sc, V, Mn, Co, Cu, and Mo, using 1000 ppm atomic absorption spectroscopy (AAS) standard solutions. The total amount of added trace elements was <0.25 wt% for experiment 1 and <0.70 wt% for all other experiments. The resulting mixture was remelted for 10 minutes at 1550 °C to promote starting material homogeneity for major and trace elements. The starting material was ground under ethanol one final time for one hour in an agate mortar, dried in air and stored at 110 °C.

Table 2 gives an overview of experimental conditions used in this study. High *P-T* experiments were conducted in an end-loaded piston-cylinder (PC) at the Faculty of Earth and Life Sciences, VU University Amsterdam, using a ½ inch diameter talc-pyrex cell assembly. The assembly was calibrated via the albite to jadeite plus quartz and fayalite to ferrosilite plus quartz transitions at 1000 °C, resulting in a pressure correction due to friction of 3%. A hand-machined graphite bucket, with an ID of 0.7 mm, OD of ~1.7 mm and length of 3-4 mm, was filled, closed with a graphite lid and inserted in a Pt capsule, with an ID of 1.7 mm, OD 2.0 mm, and length of 5-7 mm. The bottom of the Pt capsule was triple crimped, flattened and welded shut at one end, after the graphite capsule was inserted the other end was crimped and welded shut using a Lampert PUK 3 welder. Before

Table 2. Summary of experimental conditions and run products. Run products from experiments in bold were selected for trace element concentration analysis. Abbreviations: ilm: ilmenite; gk: geikielite; arm: armalcolite; opx: orthopyroxene; rut: rutile; cpx: clinopyroxene, tr: trace.

Run	Temperature (°C)	Pressure (GPa)	Time (h)	Modal abundances*
1	**1300**	**1.1**	**26**	**16% Ilm/Gk, 5% Arm, 18% Opx, 61%melt**
2+	1300	1.1	26	100% melt
3	**1305**	**1.4**	**24**	**17% Ilm/Gk, 1% Arm, 18% Opx, 64% melt**
4	**1315**	**1.7**	**23**	**20% Ilm/Gk, 23% Opx, tr Rut, 57% melt**
5	1300	2.25	22.75	32% Ilm/Gk, 5% Rut, 55% Cpx + Opx, 8% melt
6	1325	2.25	26	32% Ilm/Gk, 4% Rut, 50% Cpx + Opx, 14% melt
7	1350	2.25	26	9% Rut, 18% Opx, 73% melt
8	1400	2.25	23	13% Opx, tr Rut, 86% melt

Numbers in parentheses indicate one standard deviation (1σ) of replicate analyses in terms of last significant numbers: 30.4(4) should be read as 30.4 ± 0.4.

closing and welding shut, the capsules were held at 575 °C for ~10 min to drive off residual moist. *T* was monitored and controlled during experiments using a $W_{97}Re_3$-$W_{75}Re_{25}$ (type D) thermocouple and Eurotherm 2404 controller. The centre of the sample was located in the hotspot of the assembly, ~2 mm away from the thermocouple tip end. This ensured *T* to be within 10 °C of the thermocouple readings (Watson et al., 2002). The 'hot piston in' technique was used to bring the sample to the desired *P-T* conditions. Experiments were terminated by shutting off the power to the furnace.

Experimental run products were mounted in epoxy resin, polished and carbon coated for electron microprobe analysis. Glasses and crystals were analysed for major elements with a JEOL JXA 8800M electron microprobe at VU University Amsterdam. The accelerating voltage was 15 kV at a beam current of 25 nA. For the glass analysis we used a defocused beam of 10 μm diameter. A focused beam of 0.5 μm diameter was used for the mineral phases. Analyses were calibrated against primary standards diopside (Mg, Si, Ca), ilmenite (Ti, Fe), and corundum (Al). A natural MORB glass (for Mg, Al, Si, Ca, Fe), diopside (for Mg, Ca, and Al) and ilmenite (for Ti) were used as secondary standards. Peak and background count times were 25 and 25 s (2 x 12.5 s) respectively, while iron was measured using 36 and 36 s (2 x 18 s). Data were corrected according to the ZAF algorithm (Reed, 2005).

Trace element concentrations in crystals and glasses in experiments, containing sufficiently high proportions of silicate melt were determined by laser ablation inductively coupled mass spectrometry (LA-ICP-MS) at Utrecht University. The LA-ICP-MS system consists of a 193-nm GeoLas 200Q Excimer laser ablation system (Günther et al., 1997) coupled to a Thermo Finnigan Element 2 sector field ICP-MS instrument, operated in low-resolution mode. Samples were ablated to produce 20 or 30 μm diameter craters, dependent

on crystal size. A constant fluence of 5 J cm^{-2} was used with a pulse repetition rate of 5 Hz for both glass and co-existing minerals. Calibration was performed against NIST SRM 610 glass using the published values of Pearce et al. (1997). ^{47}Ti concentrations as obtained by electron microprobe were used as internal standard**.** The following isotopes were measured ^{45}Sc, ^{47}Ti, ^{51}V, ^{53}Cr, ^{55}Mn, ^{59}Co, ^{63}Cu ^{89}Y, ^{90}Zr, ^{93}Nb, ^{95}Mo, ^{137}Ba, ^{139}La, ^{140}Ce, ^{146}Nd, ^{147}Sm, ^{153}Eu, ^{166}Er, ^{169}Tm, ^{172}Yb, ^{175}Lu, ^{178}Hf, ^{181}Ta, ^{182}W, ^{232}Th and ^{238}U, with typical ablation times of 60 s. Background intervals of 60 s were measured before and after ablation of the sample. Trace element concentrations determined for the USGS glass external standard Columbia River Basalt BCR2-G during our analytical sessions were typically within 20% of recommended values, as suggested in the GeoReM database (e.g. Jochum and Brueckner, 2008). However, measured Er and Yb concentrations were generally >20% (up to 44%) larger than the GeoReM recommended values, but within 20% of the concentrations reported by Dorrit (2006) (3.19 and 3.25 ppm, respectively).

2.2 Lattice strain modelling

We used the crystal lattice strain model of Blundy and Wood (1994) to rationalise the measured mineral-melt partition coefficients. The model is based on the near-parabolic dependence of log(D) values for series of isovalent cations on cation radius, as first observed by Onuma et al., (1968). The lattice strain model has been applied to data for a large number of major rock-forming minerals including plagioclase (Blundy and Wood, 1991), pyroxene (e.g. Wood and Blundy, 1997; van Kan Parker et al., 2010b), and garnet (e.g. van Westrenen et al., 1999; Dwarzski et al., 2006) as well as accessory minerals including titanite (Prowatke and Klemme, 2005) and apatite (Prowatke and Klemme, 2006).

The model of Blundy and Wood (1994) describes mineral-melt trace element partition coefficients for a series of isovalent elements i ($D_i^{mineral\text{-}melt}$) with radii r_i entering a given crystal-structural site using three parameters: D_0, the maximum partition coefficient for a (fictive) element with ideal radius r_0 that imposes minimal strain on the crystal lattice when incorporated, and the site's apparent Young's modulus (E):

$$D_i^{\text{mineral-melt}} = D_0 \exp\left(\frac{-4\pi E N_A [\frac{1}{2} r_0 (r_i - r_0)^2 + \frac{1}{3}(r_i - r_0)^3]}{RT} \right) \quad (1)$$

with N_A Avogadro's number and R the gas constant.. Experimental results were fitted to Eq. 1, using a non-linear least square Levenberg-Marquardt fitting routine (Press et al., 1992). Data were weighted using the standard deviation on D as weighting factor and minimising $\chi^2 = \Sigma [(D_i^{observed} - D_i^{calculated})/ D_i^{observed}]^2$.

3. RESULTS

3.1 Run products

Run products are listed in Table 2, and major element compositions of the co-existing mineral and melt phases are given in Table 3. A schematic phase diagram for our starting material at pressures between 1.1 and 2.3 GPa and temperatures between 1300 and 1400 ºC is given in Fig. 2, with back-scattered electron images of run products shown in Fig. 3. The 'sweet spot' for suitable *P-T* conditions in experiments with this starting composition is limited. In our experiments armalcolite is found to co-exist with ilmenite and orthopyroxene at 1.1 GPa - 1300 °C and 1.4 GPa - 1305 °C (Fig. 2). Consistent with previous studies (Friel et al., 1977; Thacker et al., 2009) we find that at $P > 1.4$ GPa armalcolite is no longer stable. In three of the eight experiments, at pressures between 1.1 and 1.7 GPa, sufficient amounts of ilmenite (Ilm) and armalcolite (Arm) and melt (57-64 wt% modal abundance based on mass balance) were present to enable determination of trace element partition coefficients. In the other five experiments (at pressures of 1.1 and 2.3 GPa) either no Ilm or Arm crystals were present (with rutile becoming the stable high-Ti phase towards higher *P* and *T*), or temperatures approached those of the solidus for this composition, leading to insufficient melt for reliable *D* determination.

With increasing *P* rutile co-exists with Ilm, orthopyroxene (Opx) and/or clinopyroxene. Experiments at 2.3 GPa show that at $T > 1325$ °C clinopyroxene and Ilm are no longer stable. At $T > 1350$ °C the modal abundance of rutile decreases significantly and at 1400 °C Ti in the starting material is incorporated in the silicate melt and co-existing Opx.

Table 3. Summary of microprobe analyses (wt%) of selected experiments, *n.* is number of microprobe analysis. Other abbreviations are as in table 2. Rutile was not analysed.

Exp.	mineral	*n.*	SiO_2	TiO_2	Al_2O_3	FeO	MgO	CaO	Total
1	Ilm	8	0.03(2)	57.9(2)	0.66(2)	32.3(1)	10.2(1)	0.11(3)	101.2(2)
	Arm	11	0.14(1)	73.3(5)	2.30(11)	15.8(1)	8.89(8)	0.17(7)	100.6(4)
	Opx	9	55.0(4)	1.69(17)	1.69(25)	13.2(3)	28.1(4)	1.52(17)	101.2(1)
	Melt	21	35.9(6)	20.0(7)	6.21(29)	20.4(3)	8.97(21)	9.63(27)	101.1(2)
3	Ilm	9	0.04(1)	57.0(2)	0.78(2)	32.3(2)	10.4()	0.08(1)	100.5(4)
	Arm	13	0.16(2)	71.9(4)	2.65(3)	16.0(3)	8.96(11)	0.13(9)	99.8(6)
	Opx	11	54.3(7)	1.53(12)	1.97(23)	13.7(1)	27.7(3)	1.72(15)	100.9(5)
	Melt	8	32.4(1)	22.6(2)	5.67(4)	20.9(2)	8.58(7)	8.71(11)	98.9(3)
4	Ilm	12	0.05(2)	57.3(3)	0.93(1)	33.1(2)	9.48(15)	0.12(3)	101.0(3)
	Opx	10	53.4(6)	1.63(23)	2.36(44)	14.3(2)	26.6(3)	2.22(9)	100.5(7)
	Rut	-							
	Melt	6	32.2(6)	23.7(5)	6.25(15)	21.1(6)	7.17(88)	9.68(20)	100.1(6)

Numbers in parentheses indicate one standard deviation (1σ) of replicate analyses in terms of last significant numbers: 0.03 (2) should be read as 0.03 ± 0.02.

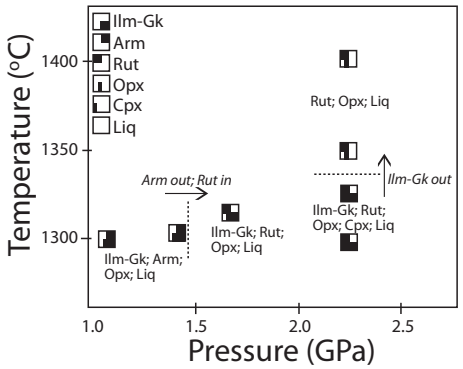

Figure 2. Phase diagram for the experimental composition, at ~IW fugacity.

Titanium-rich minerals varied considerably in size within and between experiments and were roughly between 10 and 100 μm in diameter. The largest crystals were produced in experiment 1, 1.1 GPa - 1300 °C, and crystal faces were generally well-formed. Arm crystals were generally better developed compared to Ilm crystals. Opx crystals generally also enveloped minute Ilm crystals, and showed poorly defined crystal faces. Crystals were mainly concentrated near the bottom of the experimental charge indicating crystal settling had occurred during the experiments (Fig. 3). Additionally the bottom of the charge is slightly colder.

The formed minerals did not show evidence of zoning, and glasses were transparent and free of inclusions and bubbles. Locally the melt showed a slightly quenched texture (darker areas/spots in Fig. 3). Microprobe analyses showed homogeneous concentrations with small standard deviations in both melt and minerals (Table 3).

The ilmenite crystals formed in the experiments were solid solutions between compositional end-members ilmenite ($FeTiO_3$) and geikielite (Gk; $MgTiO_3$) and are hereafter referred to as Ilm-Gk. Most lunar ilmenites are also Ilm-Gk solid solutions (e.g. Lucey et al., 2006). Mineral major element compositions do not vary significantly across the relatively limited *P-T* range covered in this study. At P = 1.1 GPa, T = 1300 °C, Ilm-Gk with composition $Ilm_{64.0}Gk_{36.0}$ coexists with Opx, $En_{76.8}Fs_{20.2}Wo_{3.0}$. At P = 1.4 GPa, T = 1305 °C, $Ilm_{63.6}Gk_{0.36.4}$ coexists with $En_{75.6}Fs_{21.0}Wo_{3.4}$ and finally at P = 1.7 GPa, T = 1315 °C, $Ilm_{66.2}Gk_{33.8}$ coexists with $En_{73.5}Fs_{22.1}Wo_{4.4}$.

3.2 Partition coefficients

Major element partition coefficients show a minor decrease with increasing P for D_{Ti} for both Ilm-Gk, from 2.9±0.1 (Exp. 1, 1.1 GPa) to 2.5 ± 0.1 (Exp. 3, 1.4 GPa) to 2.4 ± 0.1 (Exp 4, 1.7 GPa) and Arm, from 3.7 ± 0.1 (Exp. 1, 1.1 GPa) to 3.2 ± 0.1 (Exp. 3, 1.4 GPa). However, D_{Al}, D_{Mg} and D_{Si} all show slight increases with P. Mg is compatible in both Ilm-Gk (D = 1.1-1.3 ± 0.1) and Arm (D = 1.0 ± 0.1), whereas Fe is compatible in Ilm-Gk (D = 1.5-1.6 ± 0.1) and slightly incompatible in Arm (D = 0.76-0.78 ± 0.01).

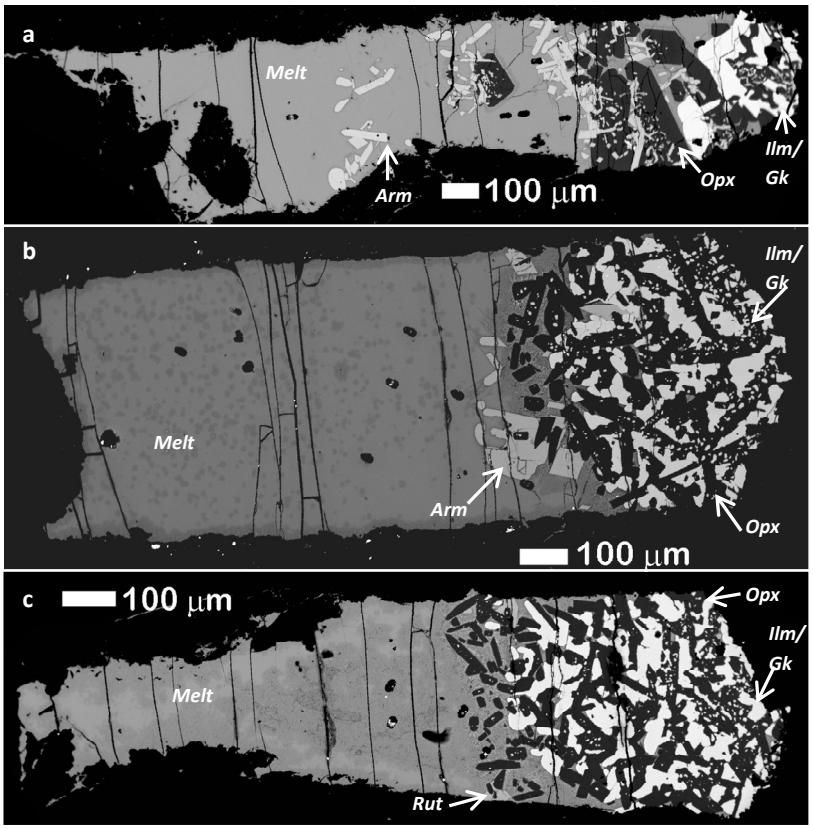

Figure 3. Back-scattered electron (BSE) microprobe images of experiments in which ilmenite formed **a**) experiment 1 at *P* = 1.1 GPa, *T* = 1300 °C; **b**) Experiment 3 at *P*= 1.4 GPa, *T* = 1305 °C, **c**) Experiment 4 at *P* 1.7 GPa, *T* = 1315 °C. Thermocouple junction (top of capsule) is towards the left of the picture in all cases. Vertical cracks are due to decompression after completion of the experiments. All experiments contain varying amounts of Ilmenite-Geikelite (Ilm/Gk) crystals and Orthopyroxene (Opx), additionally experiments 1 and 3 contain Armalcolite (Arm). Experiment 4 contains trace amounts of rutile (Rut). Darker patches are areas where the melt showed a slightly quenched structure.

Trace element concentrations of the glasses were measured on 5-8 different spots. Five or six laser ablation spots were located on Ilm-Gk crystals, four to five on Arm. Mixing between phases during laser ablation analysis was monitored using LREE concentrations and results affected by mixing (due to poor targeting of the laser beam) were discarded. Measurements were also discarded when minerals were analysed for less than 10 s, (e.g. when the mineral proved to be too thin and too few scans could be used for averaging the values, resulting in large standard deviations for individual measurements). Trace element concentrations in minerals and co-existing melts are summarised in Table 4. We were unable to use any of the analysis performed on Ilm-Gk minerals of experiment 4 at 1.7 GPa and 1315 °C, but for completeness, an average glass analysis for this experiment is given in Table 4.

Table 4. Measured trace element concentrations by laser ablation from melt and crystals, *n.* stands for number of analyses. Ti was used as internal standard.

Exp.	1			3			4
Phase	Melt	Ilm/Gk	Arm	Melt	Ilm/Gk	Arm	Melt
n.	5	5	3	6	3	3	8
Sc	27(2)	25(2)	44(2)	313(12)	228(6)	471(14)	321(29)
V	31(6)	133(9)	290(26)	64(5)	267(21)	440(32)	66(7)
Cr	60(8)	428(28)	384(37)	58(7)	451(60)	388(54)	62(12)
Mn	80(12)	94(7)	27(1)	123(13)	132(33)	41(13)	142(24)
Co	19(4)	48(2)	24(1)	61(9)	143(49)	64(12)	64(11)
Cu	2.3(4)	6.9(1)	9.2(6)	1.7(5)	4.0(4)	3.8(8)	-
Y	36(4)	0.88(23)	0.70(36)	227(28)	2.8(2)	1.9(4)	296(34)
Zr	44(4)	10(1)	26(3)	116(14)	19(2)	63(7)	161(16)
Nb	33(4)	17(2)	23(1)	94(11)	38(1)	63(10)	123(12)
Mo	39(4)	36(8)	34(5)	170(24)	101(10)	117(23)	194(19)
Ba	320(45)	1.1	3.3(10)*	545(64)	0.75	1.7(1)	740(68)
La	162(22)	0.48(18)**	1.2(7)*	432(44)	0.44(15)*	1.1(2)	575(48)
Ce	124(18)	0.24(16)	1.2(5)*	344(39)	0.21(14)	1.0(2)	448(40)
Nd	79(8)	BD<0.19	0.67(16)*	338(36)	0.26(13)	1.1(4)	451(49)
Sm	42(8)	0.37	BD<0.30	236(27)	0.61(21)*	BD<0.8	316(31)
Eu	46(9)	0.21(8)	0.58(14)*	247(33)	0.38(16)	0.69(20)	323(33)
Er	36(7)	1.1(4)	0.54(6)*	186(23)	3.5(5)	2.3(5)	244(31)
Tm	104(22)	4.6(10)	1.9(2)*	181(17)	5.2(3)	2.9(1)	245(31)
Yb	81(17)	4.8(10)	2.3(4)	199(17)	8.9(11)	4.6(6)*	270(28)
Lu	72(12)	5.7(11)	3.5(12)	182(17)	11(1)	5.8(2)	252(28)
Hf	35(5)	11(0)	29(2)	111(9)	25(5)	77(8)	154(16)
Ta	29(2)	24(2)	29(1)	93(8)	58(7)	81(5)	103(10)
W	126(19)	5.5(10)	8.2(13)*	458(53)	16(1)	27(4)	604(49)
Th	396(69)	0.82(54)	2.8(13)*	963(103)	0.42(22)*	2.5(6)	1369(95)
U	237(38)	1.2(5)	2.5(7)*	334(35)	0.63(15)	1.5(3)	445(23)

Numbers in parentheses indicate one standard deviation (1σ) of replicate analyses in terms of last significant numbers: 27(2) should be read as 27±2. When a value lacks 1σ then only 1 measurement was above the detection limit, *indicates that 1 measurement was discarded, e.g. when $n = 5$ and a number is marked by * only 4 measurements could be used. For ** 2 measurements were discarded. BD = below detection limit.

Trace element concentrations show very small variations within the different run product phases with standard deviations typically ~10% of the average value (Table 4). Higher concentrations (e.g. >10 ppm) on average correlate with smaller standard deviations (<10%), while low concentrations (e.g. <1 ppm) show standard deviations of ~30%. Uncertainties for the HREE and Th can be higher, with standard deviations of up to 65% for Th in Ilm-Gk (Experiment 1).

Resulting mineral-melt partition coefficients for Ilm-Gk and Arm are listed in Table 5. In Fig. 1 our results are compared to literature data for both Ilm-Gk and Arm. Our

Table 5. Calculated partition coefficients for Ilm-Gk and Arm and for Ilm-Gk and Arm (Experiment 1 and 3).

Exp.	1		3	
Phase	**Ilm-Gk**	**Arm**	**Ilm-Gk**	**Arm**
Sc	0.94(11)	1.65(2)	0.73(3)	1.5(1)
V	4.2(8)	9.2(19)	4.2(5)	6.9(7)
Cr	7.1(10)	6.4(10)	7.8(14)	6.7(12)
Mn	1.2(2)	0.34(5)	1.1(3)	0.34(11)
Co	2.5(5)	1.2(2)	2.3(9)	1.0(25)
Cu	2.9(7)	3.9(8)	2.3(7)	2.2(7)
Y	0.024(7)	0.019(10)	0.012(2)	0.0086(22)
Zr	0.23(3)	0.58(8)	0.17(3)	0.54(9)
Nb	0.52(9)	0.68(8)	0.40(5)	0.67(13)
Mo	0.93(24)	0.89(16)	0.60(10)	0.69(16)
Ba	0.035	0.010(3)	0.0014	0.0032(4)
La	0.0030(12)	0.0071(43)	0.0010(4)	0.0025(5)
Ce	0.0020(14)	0.010(4)	0.00062(42)	0.0029(6)
Nd	<0.0024	0.0085(24)	0.00077(39)	0.0032(12)
Sm	0.0089	<0.0071	0.0026(9)	<0.0034
Eu	0.0045(21)	0.013(4)	0.0015(7)	0.0028(9)
Er	0.030(14)	0.015(3)	0.019(4)	0.012(3)
Tm	0.044(14)	0.018(5)	0.028(3)	0.016(2)
Yb	0.059(17)	0.029(8)	0.0045(7)	0.023(3)
Lu	0.079(21)	0.049(19)	0.058(10)	0.032(3)
Hf	0.33(5)	0.83(13)	0.23(5)	0.69(9)
Ta	0.83(10)	0.99(9)	0.62(9)	0.86(10)
W	0.044(10)	0.065(14)	0.034(5)	0.058(12)
Th	0.0021(14)	0.0070(36)	0.00043(23)	0.0026(7)
U	0.0050(24)	0.011(3)	0.0019(5)	0.0046(10)

Numbers in parentheses indicate one standard deviation (1σ) of replicate analyses in terms of last significant numbers: 0.94(11) should be read as 0.94±0.11.

Ilm-Gk *D* values are generally at the lower end of the wide range of reported literature values. Armalcolite values are also generally at the lower end of the reported literature data range, however, the literature *D* range is much smaller, likely related to the relatively limited number of studies dealing with the partitioning behaviour of Arm.

D values for both minerals show an insignificant decrease with increasing *P* in the small *P* range covered by our experiments. Ilm-Gk and Arm both show an increase in incompatibility from the HREE to the LREE. Ilm-Gk and Arm show varying incompatibility of the HFSE with Th and U, and W to a lesser extent, being strongly incompatible, whilst Hf, Zr, Nb and Ta are only mildly incompatible. Both minerals preferentially incorporate U over Th. Ilm-Gk and Arm can fractionate the HFSE as $D_{Ta} > D_{Nb}$ and $D_{Hf} > D_{Zr}$. D_{Ta}/D_{Nb} is 1.54-1.59 for Ilm-Gk and 1.29-1.46 for Arm, D_{Hf}/D_{Zr} gives

1.39-1.44 for Ilm-Gk and 1.28-1.43 for Arm. Both Ilm-Gk and Arm also significantly fractionate W from Hf and D_{Hf}/D_W is 6.7-7.5 for Ilm-Gk and 11.9-12.9 for Arm. Finally for D_{Lu}/D_{Hf} we find 0.24-0.25 for the produced Ilm-Gk and 0.05-0.06 for Arm.

For the transition metals V, Cr and Cu we find $D > 1$ for both Ilm-Gk and Arm. Cr (D_{Cr} =7.5 ± 1.2) is the most compatible element in Ilm-Gk and V (D_V =8.1 ± 1.3) in Arm under these experimental conditions. A difference between Ilm-Gk and Arm is that $D_{Mn} > 1$ for Ilm-Gk, while Mn is incompatible in Arm.

3.3 Lattice strain model fits

Ilmenite-geikielite (space group: $R\bar{3}$) is characterised by a hexagonal close-packed structure of oxygens similar to the corundum structure, and consists of alternating layers of Ti- and Fe/Mg-containing octahedra (e.g. Raymond and Wenk, 1971). Both Fe/Mg and Ti lattice sites are six-fold coordinated. Armalcolite (space group: *Bbmm*) is a solid solution between ferropseudobrookite ($FeTi_2O_5$) and karrooite ($MgTi_2O_5$). Armalcolite has the pseudobrookite structure, made up of bands of distorted edge-sharing octahedra (e.g. Smyth, 1974) and is also characterised by two lattice sites referred to as the M1 site (occupied by Mg/Fe) and the M2 site (occupied by Ti), which are both six-fold coordinated.

So-called Onuma diagrams (Onuma et al., 1968) showing log(D) values versus trace element radii (six-fold coordinated values from Shannon, 1976) are shown in Fig. 4 for both Ilm-Gk and Arm for di-, tetra- and trivalent elements. Near-parabolic behaviour is clearly observed in all cases, showing that partitioning data for these minerals are amenable to crystal lattice strain model treatment. This in turn suggests the elements involved are incorporated into the Fe/Mg and/or Ti sites in both minerals. Best-fit values for lattice strain model parameters D_0, r_0 and E (Eq. 1) are summarised in Table 6 and shown as curves in Fig. 4.

3.3.1 Ilmenite-Geikielite

Divalent cations

With increasing P we find that ideal radius r_0 for M^{2+} decreases slightly from 0.781 ± 0.005 Å at 1.1 GPa, to 0.775 ± 0.002 Å at 1.4 GPa, and 0.769 ± 0.012 Å at 1.7 GPa, at a nearly constant experimental T of 1307 ± 7 °C. The error in r_0 at 1.7 GPa is slightly larger compared to the other experiments since the partition coefficient for Mn could not be determined. While r_0 increases with increasing P, E appears to decrease from 410 ± 70 GPa at 1.1 GPa to 382 ± 11 GPa at 1.4 GPa and finally to 347 ± 38 GPa at 1.7 GPa. D_0 is essentially constant at 1.57 ± 0.02 for these three experiments.

Cu and Co were not included in fitting the divalent cations since they have appreciable crystal field stabilisation energies, causing them to lie ‘off’ crystal lattice strain model parabolae (e.g. Purton et al., 2000). For Experiment 1 and 4 Ba could only be measured on one occasion. The measured values resulted in high D_{Ba} values, of 0.035 and

0.0014 respectively, and do not plot on our lattice strain fits. Our predicted values, using the lattice strain fit parameters summarised above, for D_{Ba} values are 7.1 x 10^{-20} at 1.1 GPa and 7.5 x 10^{-19} at 1.4 GPa.

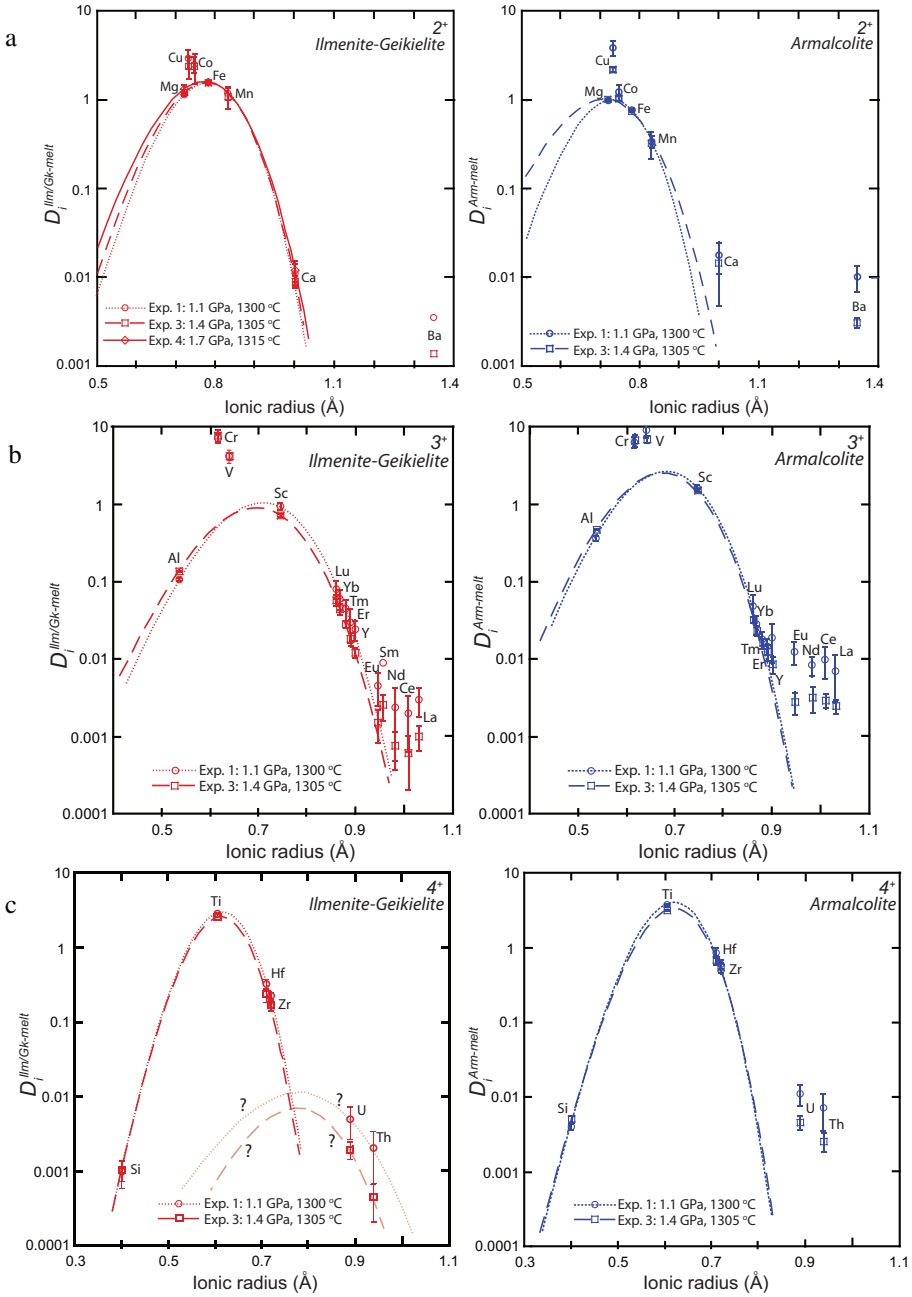

Figure 4. Onuma diagrams showing partitioning data for the Ilmenite-Geikielite (Left) and Armalcolite (Right) experiments. **a**) Divalent elements **b**) Tetravalent elements **c**) Trivalent elements.

Tetravalent cations

Si, Ti, Hf and Zr show near-parabolic partitioning behaviour with an optimum radius r_0 close to the radius of Ti (0.605 Å). D_0 shows almost no variation with pressure (2.98 ± 0.10 at 1.1. GPa, 2.56 ± 0.03 at 1.4 GPa. r_0 values are also constant t 0.616 ± 0.002 Å, and E values are indistinguishable at 1243 ± 46 GPa (1.1 GPa) and 1260 ± 32 GPa (1.4 GPa). U and Th clearly do not follow the parabolas described by the other M^{4+}. It is likely that both U and Th replace the larger Fe cation in the Ilm-Gk crystal structure rather than Ti, forming a second parabola (schematically indicated in Fig. 4b).

Trivalent cations

Partitioning data for Al, Sc, HREE and MREE show clear near-parabolic behaviour. Fitting to Eq. 1 leads to values for r_0 intermediate to those for M^{2+} and M^{4+}: r_0 = 0.708 ± 0.002 Å at 1.1 GPa, decreasing to 0.696 ± 0.001 Å at 1.4 GPa. D_0 values are comparable for both experiments at 1.05 ± 0.12 and 0.900 ± 0.043 as are E values at 447 ± 23 and 428 ± 10 GPa respectively. These values are intermediate between the E values for M^{2+} and M^{4+} elements.

3.3.2. Armalcolite

Divalent cations

For the divalent cations we find r_0 decreasing from 0.730 ± 0.007 Å at 1.1 GPa to 0.711 ± 0.027 Å at 1.4 GPa. Ideal ionic radii for divalent cations are therefore ~0.05 A smaller than for Ilm-Gk. This is consistent with the observation that in Ilm-Gk, $D_{Mg} < D_{Fe}$, whereas in Arm $D_{Mg} > D_{Fe}$. D_0 is approximately 1 for both experiments and E values average 381 GPa,

Table 6. Lattice strain best fit values for D_0, E and r_0 for Ilmenite-Geikielite and Armalcolite.

Exp.	**1**		**3**		**4**
P(GPa) T (°C)	**1.1, 1300**		**1.4, 1305**		**1.7, 1315**
Phase	**Ilm-Gk**	**Arm**	**Ilm-Gk**	**Arm**	**Ilm-Gk**
			D_0		
2^+	1.58(3)	1.00(2)	1.55(2)	1.05(3)	1.58(5)
3^+	1.08(12)	2.65(24)	0.904(43)	2.59(13)	-
4^+	2.98(10)	3.87(13)	2.56(3)	3.32(4)	-
			E		
2^+	410(70)	453(121)	382(11)	308(205)	347(38)
3^+	455(24)	536(21)	429(10)	528(11)	-
4^+	1243(46)	1014(21)	1260(38)	972(20)	-
			r_0		
2^+	0.781(5)	0.730(7)	0.775(2)	0.711(27)	0.769(12)
3^+	0.707(2)	0.682(2)	0.696(1)	0.674(1)	-
4^+	0.617(2)	0.623(2)	0.614(2)	0.621(2)	-

Numbers in parentheses indicate one standard deviation (1σ) of replicate analyses in terms of last significant numbers: 1.41(26) should be read as 1.41±0.26.

overlapping within error for the two data sets. In Arm, both Ca and Ba do not plot on our lattice strain fits and the measured values appear high compared to predicted D_{Ca} and D_{Ba}. Predicted values for D_{Ca} are 0.0088 and 0.0013 for the 1.1 GPa and 1.4 GPa experiment respectively, whilst predicted values for D_{Ba} 6.4.1 x 10^{-19} at 1.1 GPa and 1.3 x 10^{-18} at 1.4 GPa. Similar to the Ilm-Gk data sets Cu and Co were not included in fitting the divalent cations for armalcolite since they have appreciable crystal field stabilisation energies, which lead to D values that are higher than predicted for 'regular' 2^+ cations.

Tetravalent cations

Si, Ti, Hf and Zr again show near-parabolic behaviour with optimum radii centred around the radius of Ti, while U and Th do not follow this behaviour. Ideal radius r_0 is again independent of pressure at 0.622 ± 0.002 Å as is E (1014 ± 21 GPa at 1.1 GPa, 972 ± 20 GPa at 1.4 GPa). D_0 decreases slightly from 3.87 ± 0.13 at 1.1 GPa to 3.32 ± 0.04 at 1.4 GPa. Analogously to the situation in Ilm-Gk, these data indicate that U and Th enter the Arm crystal structure replacing Mg and/or Fe on the M1 site.

Trivalent cations

As we observed for Ilmenite-Geikielite, Al, Sc, and the HREE and MREE in Arm show near-parabolic partitioning behaviour leading to r_0 values intermediate between those for M^{2+} and M^{4+}. At 1.1 GPa r_0 = 0.682 ± 0.002 Å, decreasing slightly to 0.674 ± 0.001 Å at 1.4 GPa. D_0 values are identical for both experiments at 2.65 ± 0.24 at 1.1 GPa and 2.59 ± 0.13 at 1.4 GPa, as are E values at 536 ± 21 and 528 ± 11 GPa respectively.

4. DISCUSSION

4.1 Partitioning behaviour of Ilmenite versus Armalcolite

The partitioning behaviour of Ilm-Gk and Arm are compared in Fig. 5. The LREE, Th and U are all preferentially incorporated into Arm, and display lowest partition coefficients. The HREE and W show intermediate partition coefficients and are generally preferentially incorporated into Ilm-Gk, apart from W in experiment 1 at 1.1 GPa and Tm in experiment 3 at 1.4 GPa, which have somewhat higher D values for Arm. The HFSE and Mo have partition coefficients near 1, with slightly higher values for Arm. Finally the transition metals, with highest D values, show variable preference for either Ilm-Gk or Arm.

Ilm-Gk and Arm can fractionate the HFSE as $D_{Ta} > D_{Nb}$ and $D_{Hf} > D_{Zr}$. D_{Ta}/D_{Nb} is 1.54-1.59 for Ilm-Gk and 1.29-1.46 for Arm, D_{Hf}/D_{Zr} gives 1.39-1.44 for Ilm-Gk and 1.28-1.43 for Arm, consistent with Klemme et al. (2006). Both minerals significantly fractionate W from Hf: D_{Hf}/D_W is 6.7-7.5 for Ilm-Gk and 11.9-12.9 for Arm, indicating that at our experimental conditions Arm is somewhat more efficient in fractionating W from Hf. Klemme et al. (2006) found D_{Hf}/D_W values for ilmenite of 7-43. Both ilmenite and

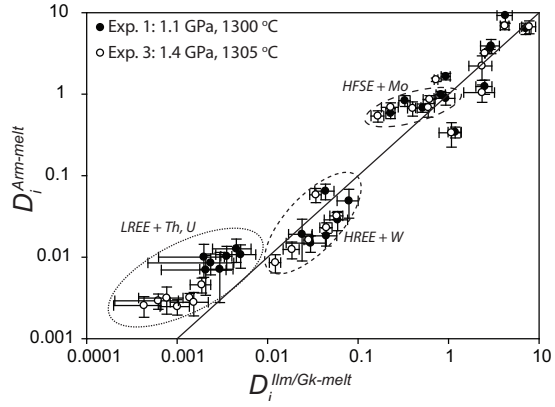

Figure 5. Mineral-melt partition coefficients of Ilm-Gk and co-existing Arm for all elements.. Unmarked elements are the transition metals.

armalcolite are therefore possible candidate causing the observed fractionation of siderophile W from lithophile Hf during lunar magma ocean crystallisation (e.g. Shearer and Papike, 1999; Lee et al., 2002; Klemme et al., 2006).

4.2 Lattice strain models

To our knowledge this is the first study using the lattice strain model of Blundy and Wood (1994) to rationalise the mineral-melt partitioning behaviour of both ilmenite-geikielite and armalcolite (Table 6; Fig. 4). As a result we are able to elucidate the lattice sites on which elements likely partition, and identify and correct for minor contamination issues affecting measured *D* values for incompatible elements.

Comparing best-fit lattice strain model parameters for Ilm-Gk and Arm shows that r_0 for divalent cations in Ilm-Gk is very close to the six-fold radius of Fe (0.78 Å, Shannon, 1976) whereas r_0 for Arm is closer to that of Mg (0.72 Å). This indicates substitution of M^{2+} into the Fe/Mg site. For both minerals r_0 for the tetravalent cations (Si, Hf and Zr) is close to that of Ti (0.605 Å), indicating that these elements preferentially substitute for Ti. For both Ilm-Gk and Arm Th and U likely substitute for the larger Fe/Mg cations.

At first glance the partitioning data for M^{3+} shown in Fig. 4c suggest a 'double parabola', implying that M^{3+} substitute into both Fe or Fe//Mg and Ti lattice sites. However, neither the Ilm-Gk nor the Arm data could be fitted to a double parabola using the lattice strain model. In addition, previous work has shown that even the smallest M^{3+} cation considered here (Al) substitutes onto the Fe/Mg site in armalcolite (Smyth, 1974), not onto the Ti site. We therefore feel that a single fit to the trivalent cations is the best available tool to describe the M^{3+} partitioning behaviour in Arm and Ilm-Gk. Resulting r_0 values are intermediate between those for M^{2+} cations on the Fe/Mg sites and M^{4+} cations on the Ti sites.

The fits to our M^{3+} data reveal a minor contamination issue with our data. The LREE clearly show higher partition coefficients than expected from the lattice strain model (Fig. 4c). As discussed by van Westrenen et al. (2001) very small (< 1 wt%) amounts of

glass contamination during trace element analysis of crystals can lead to significant overestimation of *D* values for highly incompatible elements. In Fig. 6 we show the effect of the addition of different percentages of glass to the Ilm-Gk mineral analysis for the 1.1 GPa experiment. The difference between observed and predicted *D* values for the LREE can be explained by as little as 0.1-0.3 wt% glass contamination of our mineral analyses. Fig. 6 also shows that the effect of such minor addition is minimal for the HREE.

Minor contamination during laser ablation analysis also explains the discrepancy between measured values of D_{Ba}, and for armalcolite also D_{Ca}, and values expected from lattice strain fits in both minerals. 0.3 to 0.7 wt% glass addition to the ilmenite-geikielite and armalcolite measurements are sufficient to explain the high D_{Ba} values.

Most best-fit lattice strain parameters show very little or no variation across the pressure range covered in these experiments. The only exceptions are the observed slight decreases in r_0 for divalent cations with increasing pressure for both Ilm-Gk and Arm, accompanied by small decreases in apparent site Young's moduli *E*. Decreases in r_0 with increasing *P* have been observed in partitioning data for other minerals (most notably garnet, e.g. van Westrenen and Draper, 2007; Draper and van Westrenen, 2007) and are consistent with the expected decreases in the Mg/Fe site volumes with increasing compression.

E values for divalent cations are identical within error for Ilm-Gk and Arm, and are high compared to values for M^{2+} replacing divalent major cations in other minerals, which are generally in the range 100-250 GPa. Although decreases in r_0 are often accompanied by increases in *E*, interpreting *E* values is notoriously difficult (e.g. Hill et al., 2000; van Westrenen et al., 2000a) and our data set is too small to draw definitive conclusions about the relation between r_0 and *E* for divalent cations in Arm and Ilm-Gk. *E* increases with increasing cation charge while r_0 shows a decrease. The *E* values for Arm are larger than those for Ilm-Gk in the case of trivalent trace cations, and smaller in the case of tetravalent cations.

Arm has higher D_0 values for both tri- and tetravalent cations whereas Ilm-Gk at the same conditions has higher values for the divalent cations. In Ilm-Gk D_0 decreases from the di- to trivalent cations and then increases again and shows maximum values for the tetravalent cations. For Arm D_0 shows a general increase with increasing cation charge.

4.3 Implications for Lu-Hf-Ti systematics of lunar high-Ti mare basalts

Because of the bulk composition and conditions used, the partition coefficients presented in this study are directly relevant to the Moon. Here we apply our data to assess the roles of ilmenite and armalcolite in determining the combined Lu-Hf-Ti systematics of high-Ti lunar mare basalts. A variety of models have been proposed to explain the high Ti contents of these basalts, including assimilation of late-stage ilmenite-bearing cumulates by low-Ti ultramafic liquids at shallow levels (e.g. Anderson, 1971; Hubbard and Minear, 1975; Wagner and Grove, 1997), sinking of the late stage ilmenite cumulate to form a deep hybrid

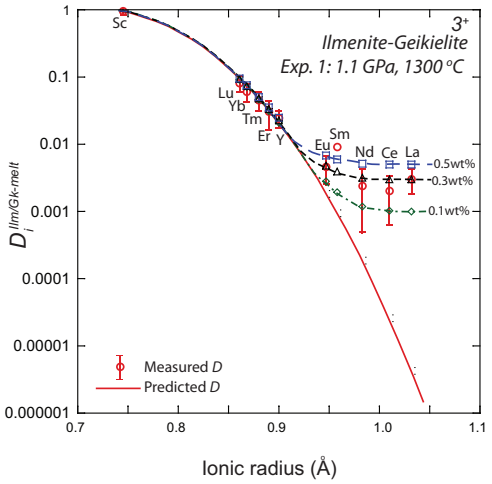

Figure 6. Onuma diagram showing predicted partitioning curve for the trivalent elements (excluding Al and Cr) for the Ilmenite-Geikielite experiment at 1.1 GPa (solid line using values from Table 6) and the calculated effect of 0.1, 0.3 and 0.5 wt% glass contamination of mineral analyses. Resulting effects on measured *D* values are large for the LREE, but minimal for the HREE. In this case, LREE D values are consistent with ~0.3 wt% glass contamination during mineral analyses.

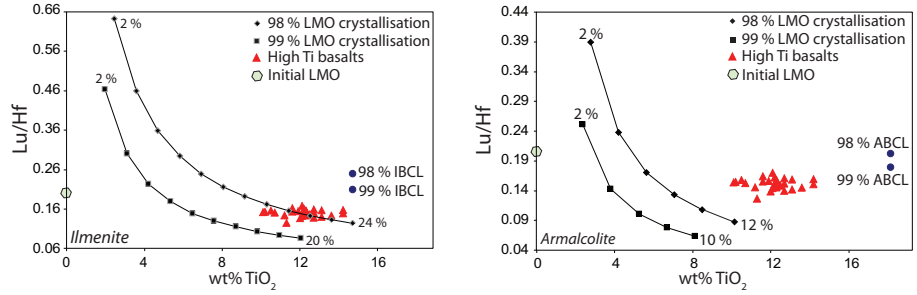

Figure 7. Comparison between observed (triangles, compilation from Beard et al., 1998 and Warner et al., 1979) and modelled (this study) Lu/Hf ratios and TiO_2 contents of high-Ti mare basalts. Curves show progressive dissolution of **a**) ilmenite-geikielite or **b**) armalcolite into 10% partial melts of early orthopyroxene cumulates. The Lu/Hf ratio of these initial melts decreases steeply with increasing Ilm **a**) or Arm **b**) addition. The Lu/Hf ratios of bulk ilmenite bearing cumulate (IBCL) and bulk armalcolite bearing cumulate (ABCL) are shown assuming Ti-rich mineral crystallisation up to either 98 or 99% total solidification of the LMO.

mantle source (e.g. Ringwood and Kesson, 1976; Hess and Parmentier, 1995) and shallow-level reaction and mixing of cumulates, followed by sinking of hybrid high-Ti material (Van Orman and Grove, 2000). In addition, Nakamura et al. (1986) and Beard et al. (1998) showed that the Lu/Hf ratios of high-Ti mare basalts (Lu/Hf = 0.12-0.17) are significantly lower than chondritic (Lu/Hf = 0.21, Lodders, 2003).

Ilm-Gk (D_{Lu}/D_{Hf} = 0.24-0.25) and Arm (D_{Lu}/D_{Hf} = 0.05-0.06) are the only minerals involved in lunar magma ocean (LMO) crystallisation that preferentially incorporate Hf over Lu. Partitioning studies of other minerals that are thought to have played a role during lunar magmatic processes all show $D_{Lu}/D_{Hf} > 1$. For example, olivine shows D_{Lu}/D_{Hf} = 3.2 (McDade et al., 2003b), clinopyroxene D_{Lu}/D_{Hf} = 2.0 (e.g. McDade et al., 2003b), plagioclase D_{Lu}/D_{Hf} = 1.8 (e.g. Tepley et al., 2010) and orthopyroxene D_{Lu}/D_{Hf} = 6.1 ± 2.5 (van Kan Parker et al., accepted MS).

Table 7. Input parameters for trace elements evolution modelling during LMO crystallization, assuming the crystallisation model of Snyder et al. (1992).

	Concentrations					
	LMO_i[1]	**High Ti[2a]**	**High Ti[2b]**	**High Ti[2c]**		
Lu (ppm)	0.119	1.0-1.1	2.4-2.6	0.5-1.5		
Hf (ppm)	0.575	6.4-7.0	14.7-15.9	5.1-10		
TiO_2 (wt%)		12.5-13.7	9.1-9.7	10.1-14.2		
Lu/Hf	**0.21**	**0.16**	**0.16-0.17**	**0.13-0.17**		
	Partition coefficients					
	D_{OL}[3]	D_{OPX}[4]	D_{CPX}[3]	D_{PLAG}[5]	D_{ILM-GK}	D_{ARM}
Lu	0.041	0.052	0.74	0.0018	0.079	0.049
Hf	0.013	0.0086	0.37	0.001	0.33	0.83
Ti	0.01	0.071	0.34	0.0446	2.9	3.7
D_{Lu}/D_{Hf}	**3.2**	**6.1**	**2**	**1.8**	**0.24**	**0.06**

Initial values for the Lu and Hf concentrations in the LMO (LMO_i = 5*CI chondrites) are derived using CI values of [1]Lodders (2003). Lu-Hf and TiO_2 concentrations from [2]Beard et al. (1998) for Apollo 17 basalts (2a) and Apollo 11 basalts (2b), and from Warner et al. (1979) for Apollo 17 basalts (2c). Partition coefficients are from [3]McDade et al. (2003b) Olivine (OL) and Clinopyroxene (CPX), [4]van Kan Parker et al. (Submitted) for orthopyroxene (Opx) and [6]Tepley et al. (2010) for plagioclase (PLAG) for which D_{Lu} was fitted using the lattice strain model. Ilm-Gk and Arm partition coefficients are from Experiment 1 (this study).

We calculated the Lu-Hf-Ti evolution of a crystallising LMO and corresponding cumulates, assuming the LMO crystallisation model of Snyder et al. (1992). Partition coefficients for all minerals involved in LMO crystallisation, including our new data, are summarised in Table 7. Following Snyder et al., (1992) we assume a 5*C1 chondrite value for initial LMO Lu and Hf concentrations.

During initial magma ocean crystallisation Lu/Hf decreases in the residual liquids due to the high D_{Lu} /D_{Hf} ratios of the crystallising minerals, and the corresponding cumulates containing Ol ± Opx ± Cpx ± Plag show superchondritic Lu/Hf ratios, between 0.36-1.2. Ilmenite and/or armalcolite start crystallising when the LMO has solidified for > 95% (Snyder et al., 1992). We test models in which the Ti-rich minerals continue crystallising up to a total of 98% or 99% total LMO crystallisation. Consistent with Snyder et al. (1992) the late stage Ti-rich minerals crystallise together with clinopyroxene and plagioclase, producing a so-called ilmenite bearing cumulate layer (IBCL) or alternatively the equivalent armalcolite-bearing cumulate layer (ABCL). Using our partition coefficients the Lu/Hf ratios of ilmenite are predicted to be subchondritic in the range 0.025-0.034, while armalcolite shows Lu/Hf ratios of 0.0068-0.0084. IBCL and ABCL vary between super- and subchondritic respectively (Fig. 7), dependant on the total amount of crystallisation of the LMO, however at ≥ 99% crystallisation, the IBCL or ABCL are not as subchondritic as the observed ratios in the high-Ti mare basalts.

Fig. 7 shows predicted Lu-Hf-Ti systematics for models whereby high-Ti basalts are generated by partially melting (10% fractional melting) the Opx cumulate formed during early LMO crystallisation, followed by shallower-level dissolution of Ilm / Arm

from late-stage cumulate remnants. When we assume Ilm-Gk crystallisation up to 98% LMO solidification, a mixture of 17% of dissolved ilmenite with 83% of cumulate partial melt is required to reproduce the observed Lu/Hf ratio of 0.16 in the high-Ti mare basalts (Fig. 7a). If armalcolite would crystallise instead of ilmenite a mixture of ~6.5% of armalcolite and ~93.5% of cumulate partial melt is sufficient (Fig. 7b). If Ti-rich mineral crystallisation from the LMO would continue up to 99% of solidification the required proportions reduce to ~9% for ilmenite and to ~3.5% if armalcolite dissolution is involved. A robust result from our modelling is that bulk dissolution of the IBCL or the equivalent armalcolite-bearing cumulate layer (ABCL) including clinopyroxene and/or plagioclase cannot reproduce the observed subchondritic Lu/Hf ratios since their Lu/Hf ratios are higher than observed in the basalts. Selective dissolution of the Ti-rich phase is therefore required, consistent with the dissolution modelling of Wagner and Grove (1997).

These scenarios reproduce the observed Lu/Hf ratio and absolute TiO_2 concentrations in the high-Ti mare basalts. Absolute concentrations for Lu and Hf in these models are lower than the measured values. Simple late-stage olivine ± orthopyroxene fractionation at shallow levels, using the partition coefficients listed in Table 7, would lead to unchanged Lu/Hf ratios and higher absolute values of both Lu and Hf. However, TiO_2 concentrations would simultaneously increase to levels far exceeding those observed.

Alternatively, fractionation of olivine ± ilmenite, or olivine ± armalcolite (as suggested by, e.g. Longhi et al., 1992) would lower TiO_2 concentrations to levels below those observed. Finally fractionation of olivine ± orthopyroxene ± ilmenite would only change TiO_2 concentrations to a very minor extend while increasing the absolute Lu and Hf concentrations. This latter scenario would also increase the Lu/Hf ratio slightly and therefore slightly more initial ilmenite dissolution would be required (18% at 98% crystallisation of the LMO, or 10% at 99% crystallisation of the LMO). We stress however that this analysis assumes that the partition coefficients listed in Table 7, chosen for their applicability during high-pressure processes, are equally valid at low pressure – an assumption that remains to be tested experimentally.

5. CONCLUSIONS

We have experimentally determined the partitioning behaviour of a wide range of trace elements between ilmenite, armalcolite and anhydrous lunar silicate melt, to constrain geochemical models of the evolution of the interior of the Moon. The lattice strain model can be applied for both ilmenite-geikielite and armalcolite to describe the partitioning behaviour for M^{2+}, M^{3+} and M^{4+} cations. Our data enable us to quantitatively model the Lu-Hf-Ti systematics of lunar high-Ti basalt. We show that the subchondritic Lu/Hf ratios, and high TiO_2 contents require preferential dissolution of ilmenite or armalcolite from late-stage

lunar magma ocean cumulates into low-Ti partial melts of deeper pyroxene-rich cumulates, followed by shallow fractionation of olivine ± orthopyroxene ± ilmenite.

ACKNOWLEDGEMENTS We like to thank Helen de Waard for assistance with the LA-ICP-MS measurements, and the VU University Amsterdam mechanical and electronic workshops for supporting the high pressure laboratory. This research was funded through a European Science Foundation EURYI award to WvW. Laser ablation ICP-MS instrumentation at Utrecht University was supported by an investment grant from the Netherlands Organization for Scientific Research (NWO).